Cellulose (2017) 24:3753–3766
DOI 10.1007/s10570-017-1379-6

ORIGINAL PAPER

High aspect ratio nanocellulose from an extremophile spinifex grass by controlled acid hydrolysis

Nasim Amiralian · Pratheep K. Annamalai · Christopher J. Garvey · Edward Jiang · Paul Memmott · Darren J. Martin

Received: 4 December 2016 / Accepted: 20 June 2017 / Published online: 26 June 2017

Abstract During the last two decades, work surrounding the preparation of a vast array of cellulose nanomaterials from both wood and non-wood based sources has steadily intensified. This study reports on the isolation of high aspect ratio nanocellulose from an arid grass source commonly called "spinifex", *Triodia pungens*, via an optimised sulfuric acid hydrolysis protocol. The unique attributes of *T. pungens* have enabled pulping and bleaching under milder conditions than used in typically reported protocols, followed by relatively easy deconstruction into nanofibres with an unprecedentedly high aspect ratio. Hydrolysis of bleached *T. pungens* under these optimised processing conditions has yielded nanocellulose with a very high aspect ratio of 144 (average dimensions of 3.45 ± 1 nm $\times$ 497 ± 106 nm), a crystallinity of 73% and a production yield of 42%. Based on the spectroscopic and X-ray scattering analyses, an unusually high content of hemicellulose (42%) is correlated with both the ease of deconstruction and the retention of nanocellulose length. This high hemicellulose content also appears to give rise to a lower transverse stiffness than previously-reported values for wood sources.

Keywords Nanocellulose (NC) · High aspect ratio · Spinifex · Acid hydrolysis · Hemicellulose · Nanofibre

Electronic supplementary material The online version of this article (doi:10.1007/s10570-017-1379-6) contains supplementary material, which is available to authorized users.

N. Amiralian · P. K. Annamalai · E. Jiang · D. J. Martin (✉)
Australian Institute for Bioengineering and Nanotechnology (AIBN), The University of Queensland, Brisbane, QLD 4072, Australia
e-mail: darren.martin@uq.edu.au

C. J. Garvey
Australian Nuclear Science and Technology Organisation (ANSTO), Lucas Heights, Sydney, NSW 2234, Australia

P. Memmott
Aboriginal Environments Research Centre (AERC), The University of Queensland, Brisbane, QLD 4072, Australia

Introduction

The concept of breaking down lignocellulosic fibres into structural components and smaller nanomaterials has recently gained intense academic and industrial interest. Due to useful chemical functionalities, high specific mechanical properties, and global abundance, nanocellulose (NC) can be potentially exploited for a large number of applications in various industries such as in light-weight materials, automotive, aerospace, paints, healthcare, energy, food, cosmetics and environmental health sectors (Kaushik and Moores 2016; Mohammadinejad et al. 2016; Moon et al. 2011b). A typical protocol for producing cellulose nanocrystals (CNCs), a common form of nanocellulose, involves (1) pulping and pre-treatment processes in order to

mechanically disintegrate the macrofibres into microfibers and to remove lignin and hemicellulose, (2) deconstruction and removal of the amorphous components by acid/enzymatic hydrolysis or oxidation, and (3) disintegration of nanocrystals by mechanical shearing or ultrasonication (Beck-Candanedo et al. 2005a; Fleming et al. 2001; Krishnamachari et al. 2012; Lavoine et al. 2012; Lin et al. 2012; Mendez et al. 2011; Paakko et al. 2007). Depending on the source of cellulose and hydrolysis conditions employed (e.g. controlled time, temperature and acid concentration), CNCs with variable morphology and property profiles can be produced (Brinchia et al. 2013; Krishnamachari et al. 2012; Peng et al. 2011; Yue et al. 2012). Typically, the isolation of CNCs via acid hydrolysis or similar protocols from lignocellulosic biomass sources like wood pulp and other non-wood pulps (e.g. cotton, sisal, flax and jute) has typically resulted in short 'rod-like' or elongated 'rice-like' nanocrystals with an aspect ratio ranging between 16 and 50 (Brinchia et al. 2013; Moon et al. 2011b; Oksman et al. 2016). In contrast, the isolation of high aspect ratio nanocellulose (typically 70–100) from rare marine creatures called tunicates (*urochordates*) has been achieved via acid hydrolysis, and these tunicate-derived NC have been successfully utilized as efficient polymer composite reinforcing nanofillers, in part due to satisfying the "critical length" criteria (Eichhorn 2011; Elazzouzi-Hafraoui et al. 2008; Favier et al. 1995; Jorfi et al. 2013a; Khandelwal and Windle 2013; Peng et al. 2011; Zhao et al. 2015). However, due to the rarity of the tunicates, their use has generally been restricted to academic research activities and the mass production of more affordable high aspect ratio nanocelluloses from plant materials via a typical acid-hydrolysis methods still remains a challenge. Herein, we address this challenge, demonstrating the successful production of high aspect ratio nanocellulose from 'spinifex grass', by using a milder pulping process and an optimised acid hydrolysis procedure.

Spinifex grasses can be traced back over 15 million years, surviving in highly drought-prone regions and low-nutrient soils, and growing predominantly in arid and semi-arid Australian grasslands which cover one-third of the continent (roughly 2.1 million km^2 in area) (Crisp et al. 2015; Toon et al. 2015). Using one of the most abundant spinifex grasses (*Triodia pungens*), we have recently reported an easy deconstruction of high aspect ratio cellulose nanofibres using a milder pulping treatment and low mechanical energy consumption. This has been attributed to the unique spinifex leaf anatomy and high hemicellulose content (Amiralian et al. 2015a, b). In this study, we investigate the impact of residual lignocellulosic components in spinifex pulp, specifically hemicellulose on the subsequent acid hydrolysis treatment. It should be noted that nanocellulose (NC) with a low aspect ratio (<100), and typically obtained via an acid hydrolysis process are commonly called 'cellulose nanocrystals' (CNCs), or have been previously referred to as 'nanowhiskers' or 'whiskers' (Abdul Khalil et al. 2014). In order to avoid confusion, the nanocellulose obtained from *T. pungens* grass herein will be described as general nanocellulose (NC). However, according to the extraction method they could be described as acid hydrolysed 'cellulose nanocrystals (CNCs)', or alternatively, based on the observed morphology it could be legitimately classified as 'cellulose nanofibrils' (CNFs).

Materials and methods

Materials

T. pungens grass material was collected from the native arid grasslands around Camooweal, Queensland, Australia (19.9°S, 138.1°E). The pulping and hydrolysis chemicals; sodium hydroxide and glacial acetic acid (Ajax Finechem, Scoresby, Australia), sodium chlorite—Technical Grade 80% (Sigma-Aldrich Castle Hill, Australia), and sulphuric acid 98% (RCI Labscan Bangkok, Thailand), were used as received.

Isolation of NC from T. pungens via acid hydrolysis

T. pungens bleached pulp was prepared using the methods we described previously (Amiralian et al. 2015a). Briefly, washed and ground grass was firstly delignified with a 2% (w/v) sodium hydroxide solution at a solvent to solid ratio of 10:1 and a temperature of 80 °C for 2 h, followed by bleaching with a 1% (w/v) acidic solution of sodium chlorite at 70 °C for 1 h and at a solvent to solids ratio of 30:1. The lignocellulosic composition of water washed spinifex grass and bleached pulp were analysed using the standard

methods (TAPPI T-222 om-88, 2006; TAPPI UM-250, 1991), as also described in our previous work (Amiralian et al. 2015b).

With the aim of optimising the acid hydrolysis protocol for producing CNC, the bleached pulp was treated with a sulphuric acid solution at various concentrations (35–50% (v/v)), different temperatures (45 and 50 °C) and times (1, 3 and 6 h). After hydrolysis, the fibre dispersions were centrifuged for 20 min at 4750 rpm 4 times in order to remove the excess acid and dissolved extractables. Subsequently, the resultant precipitate was dialysed in deionised water for one week and then re-suspended in deionised water using an ultrasonic probe (Q500 Sonicator, QSonica Newtown, United States) set at 25% amplitude, with a frequency of 20 kHz and an output energy of 500 W for 20 min. The efficiency of the process was evaluated by measuring the production yield and visual appearance. The approximate production yield of NC was calculated using the Eq. (1):

$$Yield\% = \frac{Dry\ weight\ of\ nanocellulose\ (g)}{Dry\ weight\ of\ bleached\ fibre\ (g)} \times 100 \quad (1)$$

where the dry weight of samples was measured after drying in a convection oven at 105 °C until a constant weight was obtained.

Attenuated total reflectance (ATR) fourier transform infrared spectroscopy (FT-IR)

In order to understand the chemical composition and functionalities of the *T. pungens* samples, Fourier transform infrared spectroscopy was performed on a Thermo-Nicolet 5700 ATR FT-IR spectrometer equipped with a Nicolet Smart Orbit single bounce, diamond ATR accessory (Thermoelectron Crop., Waltham, USA). Dried samples were directly pressed on the diamond internal reflection element of the ATR accessory and spectra were recorded in the wavenumber range of 4000–500 cm^{-1} and a resolution of 4 cm^{-1} for 128 scans.

Transmission electron microscopy (TEM)

TEM images of the nanocellulose from aqueous suspension were obtained using transmission electron microscopy (JEOL 1011 TEM—JEOL Pty Ltd., Frenches Forest, Australia) at 100 kV. Samples were prepared by depositing 1 µl of NC dispersion on a glow discharged formvar-coated 200 mesh copper/palladium grid (ProSciTech, Queensland, Australia). After drying at room temperature, samples were stained with a 2% uranyl acetate aqueous solution (UA) for 10 min. The average diameter and length of nanocellulose fibres were determined using digital image analysis (Image J). For each sample, 250 measurements were randomly selected and measured from several TEM images with the same magnification.

Thermogravimetric analysis (TGA)

The thermal stability of nanocellulose was measured using a TGA/DSC1-thermogravimetric analyser (Mettler Toledo, Tennyson, Australia) in the temperature range of 25–500 °C with a constant heating rate of 10 °C/min under nitrogen atmosphere.

X-Ray diffraction (XRD)

The crystalline structure of dry samples was examined by X-ray diffraction analysis conducted on a Bruker D8 Advance X-ray diffractometer (Bruker, Karlsruhe, Germany) with a 0.2 mm slit. Graphite-filtered Cu-Kα radiation (wavelength = 1.54 Å) was generated at 30 kV and 20 mA with a sample scanning range between 2θ = 5° and 40° at a speed of 1°/min. The crystallinity index was measured using Eq. (2) (Segal et al. 1959):

$$\mathrm{CrI} = ((I_{200} - I_{\mathrm{am}})/I_{200}) \times 100 \quad (2)$$

where I_{200} represents the intensity of the peak at 2θ = 22.4°, which is the main peak for the crystalline phase, containing both amorphous and crystalline domains, and where I_{am} represents the amorphous domain and correlates with the intensity of the peak at 2θ = 18.6°, which is the valley (minimum) between the crystalline peaks of cellulose polymorph Iβ 1–10 (15°), 110 (16.6°) and 200 (22.4°) planes (French 2014; Qing et al. 2013; Sheltami et al. 2012).

The mean size of crystalline regions was calculated using the Scherrer equation (3) (French and Santiago Cintron 2013; Scherrer 1918):

$$\mathrm{D} = \frac{\kappa\lambda}{\beta\cos\theta} \quad (3)$$

where K is the shape factor and is approximately = 0.89, β is the line width in radians at half the maximum intensity of I_{200}, λ is the wavelength of the radiation (0.154 nm) and θ is the scattering angle of the peak (200).

Small angle X-ray scattering (SAXS)

SAXS measurements were carried out on a Bruker Nanostar (Bruker, Karlsruhe, Germany) operating on a rotating anode X-ray source to provide CuKα X-rays (wavelength, λ = 1.54 Å). Using the calibrated beam centre position, a 68 × 68 micron pixel size on the 2-D detector and a 72 cm from sample to detector distance to define the measurement geometry, the counts per detector pixel were converted to intensity versus q, the scattering vector, where $q = 4\pi.sin(\theta)/\lambda$, and θ is the scattering angle. This was achieved using the Nika macros for IgorPro (Ilavsky 2012). The effective *q* range of these measurements was 0.012–0.39 Å, which covers the approximate size of elementary cellulose crystallites (Garvey et al. 2005). Samples were packed into 1.5 mm quartz capillaries (Charles Supper, Natick, MA, USA) and the scattering from an empty capillary was subtracted as the appropriate sample background.

Amplitude modulation–frequency modulation (AM–FM) atomic force microscopy (AFM)

The transverse elastic modulus of individual nanocellulose fibres was measured by amplitude modulation-frequency modulation (AM–FM) (Amiralian et al. 2015b). All topography images have been obtained from a dried drop of very dilute dispersion of NC on a glass slide using a Cypher S AFM (Asylum Research/Oxford Instruments, Santa Barbara, CA) in air. The cantilevers, Tap 300 probes (Budget Sensors, Bulgaria), were used with a nominal resonance frequency of 300 kHz and a nominal spring constant of 40 N/m. All probes were mounted in a high frequency/low noise AM–FM cantilever holder. For the AM pass, probes were actuated to a free air amplitude of 1.5 V, at the nominal resonant frequency and engaged at an 800 mV set point. The second pass involved actuating for the second harmonic at approximately 2 MHz for a free air amplitude of 100 mV while maintaining the phase to 90 degrees, and probe tapping was in a repulsive mode at a phase less than 50 degrees.

Results and discussion

Optimisation of acid hydrolysis

In a typical published procedures for producing nanocellulose from pure cellulose by acid hydrolysis, the acid concentration generally employed is in the range of 35–70%, temperature can vary from room temperature to 70 °C (Habibi et al. 2010b; He et al. 2014; Ioelovich 2008, 2014; Saralegi et al. 2014), and the corresponding hydrolysis time can be varied from 20 min to overnight. *T. pungens* bleached pulp with a high residual hemicellulose (42 wt%) and relatively low lignin content (3 wt%) was hydrolysed at 45 °C and 50 °C using different sulphuric acid concentrations and various hydrolysis times. Table 1 summarises the production yield and the visual appearance of dried NC samples isolated following these different hydrolysis conditions. *T. pungens* pulp containing non-cellulosic residuals (e.g. hemicellulose and lignin), which are associated with a different reactivity to sulphuric acid, understandably has a more complex structure than the pure cellulose, therefore, the hydrolysis process for this starting material is not a simple and clear reaction pathway. With an increase in the concentration of sulphuric acid, the colour of NC samples changed from white to yellow and then deep brown due to the dehydration or carbonisation reactions of hemicellulose, lignin, and cellulose (Ioelovich 2008). Under more aggressive hydrolysis conditions (e.g. 50% and 45% (v/v) sulphuric acid for 3 h at 45 °C), the crystalline structure of cellulose fibres was disrupted through the sulphuric acid interference with hydrogen bonding, and breakdown the cellulose structure into the oligosaccharides (Ingegerd et al. 1995). The yield of NC obtained under these conditions was negligible.

Using a lower concentration of sulphuric acid [35% (v/v)], but increasing the digestion temperature from 45 to 50 °C, or alternatively increasing the digestion time to 6 h, appears to have also promoted the hemicellulose dehydration reactions to produce slightly yellowish NC. It was found that the optimised conditions for the isolation of high yield (about 42%) nanocellulose from spinifex pulp, with its higher residual hemicellulose content, required a combination of lower temperature and acid concentration. For example, 40% (v/v) sulphuric acid at 45 °C for 3 h.

Table 1 Effect of acid concentration, time and temperature on the yield and appearance of *T.pungens* NC

Acid concentration (% v/v)	Time (h)	Temperature (°C)	Yield (%)	Appearance
35	3	45	33	White
	3	50	40	Light yellow
	6	45	43	Light yellow
40	3	45	42	White
45	1	45	8	Deep yellow
	3	45	0	–
50	1	45	<2	Deep brown

Electron micrographs TEM images displayed in Fig. 1 compare the morphology of various nanocellulose samples obtained following different acid hydrolysis conditions. It can be seen that the optimally-treated [40% (v/v), 45°C, 3 h] nanocellulose suspension contained relatively long and thin nanocellulose particles consisting of individual fibers, as well as some agglomerated bundles.

The optimally acid-hydrolysed nanocellulose sample still exhibited a slightly curved appearance like cellulose nanofibers (CNFs), rather than presenting a more typical flat, straight and rigid structure (Yoon et al. 2014). It seems that during the controlled acid hydrolysis process, amorphous hemicellulose near the surface is readily hydrolysed. Lignin slows down the cellulose hydrolysis process and condenses by

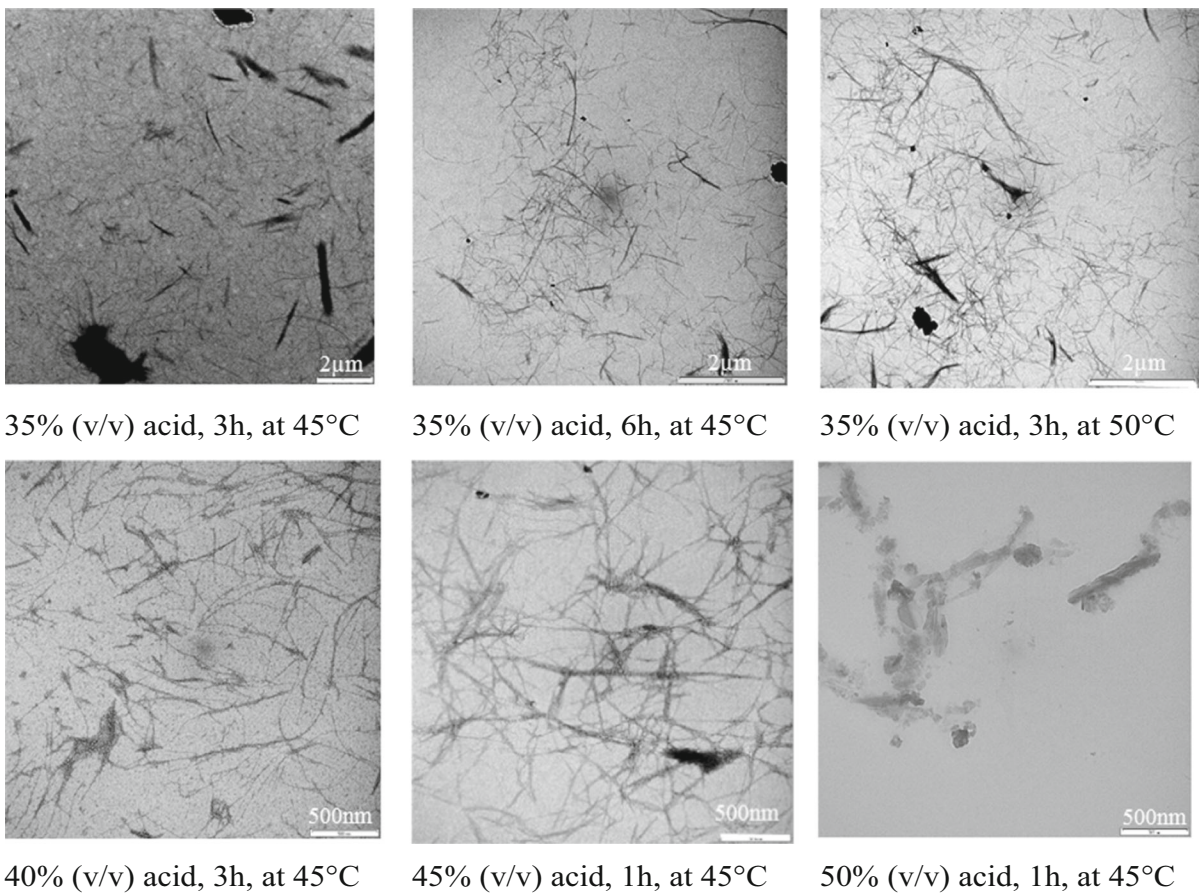

Fig. 1 TEM images of nanocellulose samples obtained from *T. pungens* using different acid hydrolysis conditions

sulphuric acid, so sulphuric acid cannot easily penetrate into the crystalline structure of fibril bundles (Ingegerd et al. 1995). Following the optimal hydrolysis conditions (40% (v/v) sulphuric acid at 45 °C, for 3 h), the resultant *T. pungens* NC had an average diameter of 3.45 ± 0.75 nm and an average length of 497 ± 106 nm. This confirms that the nanocellulose obtained via an optimised acid hydrolysis process from *T. pungens* are long and thin, with an impressive average aspect ratio of approximately 144.

Furthermore, the length of NC was retained even after this suspension was exposed to intense ultrasonic energy (at 70% amplitude for 20 min) (Fig. 2). Typically, for the production of CNC using acid digestion methodology, intense chemical treatment conditions along with more intense ultrasonication are required in order to sufficiently isolate CNC with more uniform NC widths. However, such conditions also tend to cause the breakage of the NC and consequently result in the production of short 'rod-like or elongated rice-like' cellulose nanocrystal (CNC) or whisker (CNW), with a width range of 3–15 nm and lengths in the range of 50–500 nm (Moon et al. 2011a).

Figure 3 compares the aspect ratio of NC from *T. pungens* with CNCs obtained from other sources of cellulose and using different hydrolysis conditions (Beck-Candanedo et al. 2005b; Cao et al. 2007; Elazzouzi-Hafraoui et al. 2008; Favier et al. 1995; Garcia de Rodriguez et al. 2006; Habibi et al. 2010a; Jorfi et al. 2013b; Li et al. 2009; Lu and Hsieh 2012; Rahimi and Behrooz 2011; Sacui et al. 2014). To the best of our knowledge, our optimised combination of mild pulping procedures followed by acid hydrolysis has not previously been utilised to produce high aspect ratio nanocellulose of this nature from a plant source. As communicated in Fig. 3, nanocellulose dimensions are heavily influenced by sulphuric acid treatment conditions, and when pure cellulose is used as a starting material, it results in low aspect ratio cellulose nanocrystals.

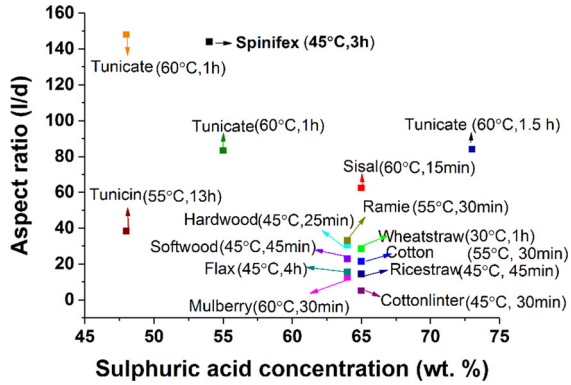

Fig. 3 Comparison of the aspect ratio of NC obtained from *T. pungens* with the other sources of cellulose using different acid hydrolysis conditions (Beck-Candanedo et al. 2005b; Cao et al. 2007; Elazzouzi-Hafraoui et al. 2008; Favier et al. 1995; Garcia de Rodriguez et al. 2006; Habibi et al. 2010a; Jorfi et al. 2013b; Li et al. 2009; Lu and Hsieh 2012; Rahimi and Behrooz 2011; Sacui et al. 2014)

The high aspect ratio of *T. pungens* NC can be attributed to the high hemicellulose content and perhaps also evolutionary aspects peculiar to *T. pungens,* which have been heavily influenced by adaptation to extreme climatic conditions (Amiralian et al. 2015b). It can be hypothesised that the hemicellulose on the surface of cellulose crystallites (Fig. 4) is more susceptible to hydrolysis than the crystalline

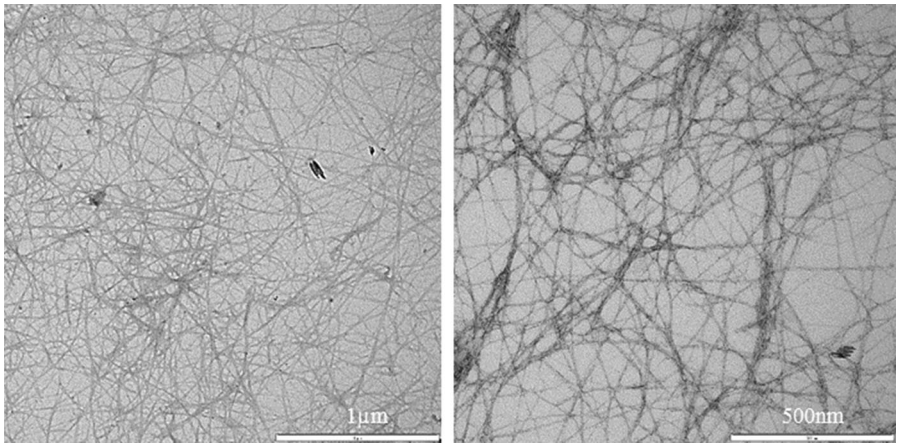

Fig. 2 TEM images (two magnifications) of *T. pungens* NC obtained from acid hydrolysis with 40% (v/v) sulphuric acid at 45 °C for 3 h, followed by ultrasonication at 70% amplitude for 20 min

cellulose chains, retaining the nanocrystals' structure without a significant disruption.

The chemical structure of T. pungens NC as discussed, traditionally pulping and bleaching processes associated with the complete or partial removal of lignin and hemicellulose are commonplace in nanocellulose preparation. These steps facilitate the subsequent ease-of-separation of cell wall components and therefore subsequent production of nanocellulose. The compositional changes upon pulping spinifex grass under milder conditions indicate that the bleached spinifex fibres retained up to 55% cellulose, 3% lignin and 42% hemicellulose. In order to follow the chemical changes upon hydrolysis, the bleached fibre and nanocellulose were studied using FTIR spectroscopy (Fig. 5). For each sample, peaks present in the region of 3000–3500 cm^{-1} indicate the strong hydrogen bonding of hydroxyl functionalities (O-H) as the principal functional group in lignocellulosic materials (Rueda et al. 2011; Yin et al. 2011b). The peaks around 700–900 cm^{-1} (C-H of aromatic hydrogen), 1108 cm^{-1} (OH of C-OH) and 1430 cm^{-1} (O-CH3 of methoxyl-O-CH3) which are assigned to the glycoside bonds and the CH_2 bending, can be observed for both bleached and acid hydrolysed fibres with less than 50% (v/v) acid concentration. These results indicate that the non-cellulosic components have not been removed completely after bleaching and acid hydrolysis.

The absorption at 813 cm^{-1} for S-O-H bonds also indicates the presence of sulphate functional groups on the NC surface after acid hydrolysis. A peak observed only in bleached fibre at around 1734 cm^{-1} is assigned

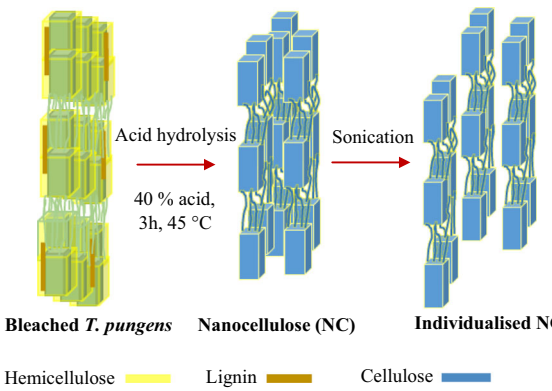

Fig. 4 Schematic representation depicting the influence of hemicellulose during hydrolysis, and enabling the retention of high aspect ratio nanocellulose

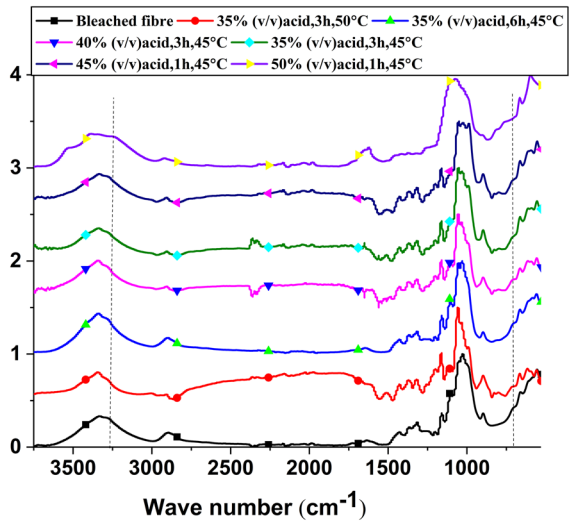

Fig. 5 FTIR spectra of *T. pungens* bleached and acid-hydrolysed samples

to the O=C–OH group of the glucuronic acid unit in hemicellulose, and indicates a split-off of the carbonyl group after acid hydrolysis (Sheltami et al. 2012). Another band around 1240 cm^{-1}, which corresponds to the axial asymmetric strain of =C–O– in ether, ester, and phenol groups of lignin and hemicellulose, is not visible in the NC spectra, which suggests that the hydrolysis conditions successfully cleaved the C–O bonds in cellulose and hemicellulose, as well as the alkyl-aryl ether bonds in lignin (Kumagai et al. 2015). Additionally, the intensity of the absorption band at 1650 cm^{-1} assigned to the absorbed water, showed an apparent decrease after acid hydrolysis, indicating that NC had a lesser ability to retain water, which is likely due to the loss of polar O–H and C=O groups from hemicellulose (Yin et al. 2011a). However, for the sample hydrolysed with 50% (v/v) acid, the characteristic peaks of glycoside bonds (891 cm^{-1}) and the CH_2 bending of C6 (1430 cm^{-1}) have disappeared indicating the partial degradation of cellulose chains (Gu and Catchmark 2012; Hayashi et al. 2005; Lu and Hsieh 2010).

Thermal stability of T. pungens NC Thermogravimetric analysis (TGA) was used to examine the influence of non-cellulosic residuals and the hydrolysis conditions on the thermal stability of *T. pungens* NC. Cellulosic fibres containing hemicellulose and lignin typically exhibit multi-step degradation behaviour in which pyrolysis has been observed to occur at

different temperatures depending on the composition of monosaccharides and lignin (Collard and Blin 2014; Yang et al. 2007). This multi-step degradation profile was observed in the bleached *T.pungens* fibres, while the acid hydrolysed NC samples showed a single-step degradation at a lower temperature, followed by charring (Fig. 6). This difference in degradation profiles can be attributed to differences in biomass constituents i.e. cellulose, hemicellulose, and lignin content. The bleached spinifex fibres showed weight losses at 150 °C [desorption of physically absorbed water), 250 °C (desorption of chemically absorbed water (Quievy et al. 2010) and/or the decomposition of hemicellulose monosaccharides (Werner et al. 2014)], and 303–500 °C (decomposition of cellulose chains (Collard and Blin 2014; Scheirs et al. 2001; Yang et al. 2007)). The acid hydrolysed samples, on the other hand, showed considerably different thermal degradation behaviour characterised by lower onset degradation temperatures (120–150 °C). As found in the other sources of cellulose (Roman and Winter 2004; Teixeira et al. 2010; Tonoli et al. 2012), the acid hydrolysis process appears to decrease the thermal stability of the resulting NCs. However, given the evidence that hemicellulose has a lower thermal stability than cellulose (Yang et al. 2007), it might be expected that the removal of hemicellulose by acid hydrolysis might lead to a higher overall thermal stability. This is not the case due to the number of sulphate groups introduced on the NC surface, which may be involved in catalysing the dehydration of glycosidic bonds at elevated temperature, leading to an earlier onset of degradation for the NC. Furthermore, previous studies have shown that an increase in acid hydrolysis time, concentration and temperature all lead to an increased number of surface sulphate groups on the NC (Roman and Winter 2004).

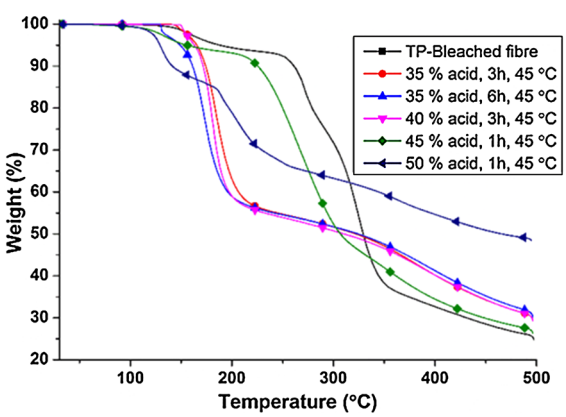

Fig. 6 Effect of hydrolysis conditions on the thermal stability of NC

For the NC samples hydrolysed for a longer time of 6 h (with 35% (v/v) sulphuric acid), the TGA curves display an earlier desorption temperature at 130°C, compared to the sample hydrolysed for 3 h. Similarly, when the concentration of sulphuric acid used for hydrolysis was increased from 35 to 40% (v/v) (for 3 h), the TGA showed an earlier degradation weight loss at around 180 °C (starting from 150°C). Furthermore, when the acid concentration was increased further to 45% (v/v) (for 1 h), the samples showed an even earlier onset degradation temperature for water desorption at 120 °C, followed by pyrolysis beginning at 210 °C (with a maximum degradation temperature of 271 °C). From these results, it is clear that a higher concentration of sulphate functionalisation on the NC surface (by increasing the hydrolysis time or concentration) appears to promote earlier dehydration reactions in the NC, leading to an earlier onset of thermal degradation. In addition to this, the high surface area of nanocellulose might also play an important role in decreasing their thermal stability due to the increased exposed surface area to reactants (Camarero Espinosa et al. 2013). Among the spinifex-derived NCs, the sample obtained after treatment with 45% (v/v) acid for 1 h, which was associated with the lowest final mass yield, showed a higher thermal stability. This can be presumably attributed to the morphology induced during the hydrolysis at high-acid concentration, under which the surface layers of microscale fibres are hydrolysed rapidly, leaving the inner (crystalline) nanofibrils unaffected. Additionally, treating cellulose at high acid concentration may also undergo other chemical transformations such as furfuralic structure formation on the surface of nanofibres (Dias et al. 2007; Dussan et al. 2015; Gonzalez et al. 1986). This may help retain a relatively high crystallinity, which may also lead to a better thermal stability. In other words, the lower degradation temperature of NC may potentially correspond with the degradation of more accessible and highly sulphated amorphous regions, whereas the breakdown of unsulphated crystalline cellulose interior occurs at a higher temperature (similar to native fibrils).

Finally, all of the acid hydrolysed NCs showed a higher residual mass at 500 °C than the bleached fibre.

This is particularly evident for the sample treated with 50% acid, which retained a mass yield of approximately 50% after pyrolysis at 500 °C. Several other authors (Henrique et al. 2015; Wang et al. 2007) have also reported higher mass yields for the pyrolysis of sulphuric acid hydrolysed CNCs compared to other forms of cellulose (Henrique et al. 2015; Wang et al. 2007). Although the reason for this difference in char yield is not completely clear, according to Austen et al. (Abraham et al. 2011), the increase in residual char and decrease in degradation temperature during the pyrolysis may be caused by an increased rate of formation of free radicals (which are promoted by the sulphate groups) and stabilised by condensed carbon ring formation in the char. As such, in regards to the thermal processability of the acid hydrolysed NC, the selection of NC type and treatment conditions will depend on the application. A 30–45% acid treatment may be beneficial if a high yielding char is required, while if a thermally stable (150–300 °C) high aspect ratio NC is required, other preparation techniques may be necessary which do not add sulphate groups to the material surface. This may include bead milling (Mohd Amin et al. 2015), ultrasonication (Lu et al. 2014) or phosphoric acid treatment (Camarero Espinosa et al. 2013).

Morphological changes aspects of NC

X-ray diffraction in order to examine the influence of the hydrolysis conditions on the crystalline structure of *T. pungens* samples, the crystallinity index was measured by X-ray diffraction (XRD). Figure 7 shows a comparison of the XRD diffraction patterns of dry NCs with bleached fibres, and Table 2 summarises the crystallinity index as well as the size of crystalline domains. The X-ray diffraction patterns for the bleached fibres, as well as all of the acid-hydrolysed NC produced using less than 45% (v/v) sulphuric acid concentration, showed characteristic peaks at around $2\theta = 15°–16.5°$ (for 1–10 and 110 and planes) and 22.4° (200 plane) which are indicative of the typical cellulose Iβ structure (French 2014; Moran et al. 2008; Qing et al. 2013; Sheltami et al. 2012).

Comparing the bleached pulp and acid-hydrolysed NCs, an increase of crystallinity was undoubtedly due to the partial removal of hemicellulose and lignin, which largely constitute the amorphous parts of the samples, leading to realignment of cellulose

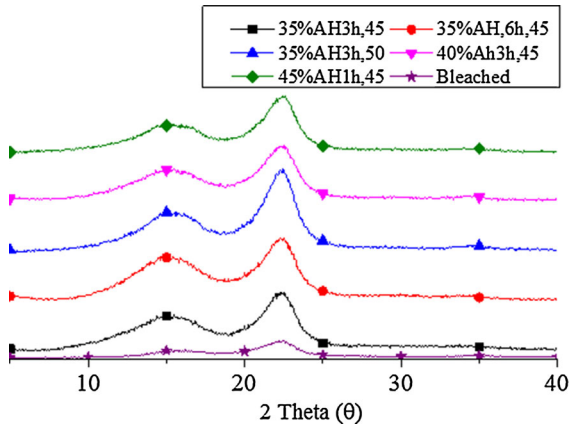

Fig. 7 X-Ray diffraction pattern of *T.pungens* bleached and acid-hydrolysed fibres

molecules. The slight increase of crystallinity also suggests that acid and water molecules are unable to penetrate into the fibril bundles under our reaction conditions, thus, the bundles must be hydrolysed through the surface reaction processes (Zhao et al. 2007). Spinifex showed the retention of crystallinity, with no significant change in the crystallite size using different hydrolysis conditions.

Small angle X-ray scattering (SAXS) a SAXS pattern for the bleached fibres and the NC obtained via an optimised acid hydrolysis process (40% (v/v), 45°C, 3 h) is shown in Fig. 8. Each dataset consists of a linear region on the log-intensity *vs.* loq-q plot superimposed on a broad peak-like feature. The slope and intensity of the linear regions of the curves indicate the size and surface roughness of the aggregates of cellulose. Because of the limited q-range of the laboratory-based SAXS measurement, it is difficult to extract information on these aspects of the fibres from these SAXS curves. The changes in the higher q range (0.1–0.3) upon hydrolysis indicate the degradation of the cell wall order and removal of material during hydrolysis. The position of the broad peak is indicative of the spatial correlation, the average distance between nano-scale cellulose (Jakob et al. 1996) and the relative intensity to the baseline the relative number of correlated/aggregated CNCs. In order to accentuate the peak with respect to the scattering due to the surface of CNC aggregates, the data was replotted as intensity xq^2 versus q following the Lorentz correction for semicrystalline polymers (inset Fig. 8) (Cser 2001).

Table 2 Crystallinity index and size of crystalline domains of *T. pungens* bleached and acid-hydrolysed fibres

Sample	Crystallinity index (%)	Crystallite size (nm)
Bleached fibre	72	4
NC (35% (v/v) acid, 3 h, 45 °C)	72	4.3
NC (35% (v/v) acid, 6 h, 45 °C)	71	4.2
NC (35% (v/v) acid, 3 h, 50 °C)	77	4.7
NC (40% (v/v) acid, 3 h, 45 °C)	76	4.7
NC (45% (v/v) acid, 1 h, 45 °C)	78	5.7

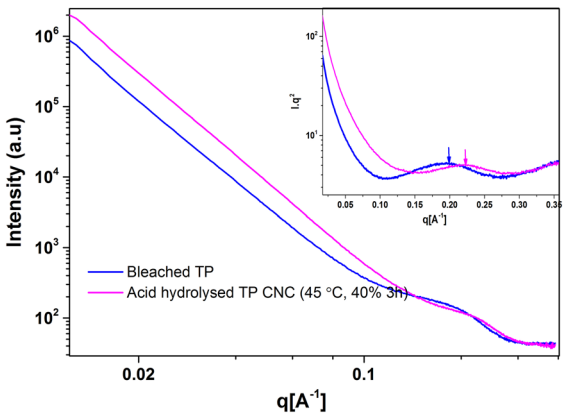

Fig. 8 SAXS profile of bleached *T. pungens* fibre and NC obtained from acid hydrolysis under optimized conditions. The *inset* shows the Lorentz-corrected data with *arrows* indicating the position of the correlation peak

The approximate peak position is shown with an appropriately-coloured arrow. Overall, upon hydrolysis the correlation peak shifts to higher values of q, shorter distances (distance $= 2\pi/q_{peak}$) and less intensity with respect to the baseline of native grass. In the case of the peak position, it shifts from 0.20 Å^{-1} which is equivalent to an average distance of 31.4 Å in the bleached fiber to 0.23 Å^{-1} which is equivalent to 27.5 Å in the case of the acid-hydrolysed nanocellulose. This peak shift indicates a decrease in the spacing between the crystalline domains. This decrease in spacing, assuming that no cellulose is degraded under mild treatments, can be the result of the removal of lignin and the amorphous polysaccharides embedded between the cellulose crystallites. This also, in turn, enhances the packing of nanocellulose together through the hydrogen bonding from free hydroxyl groups. It is also important to note that the intensity of this peak remains almost the same, even after hydrolysis. This suggests that the correlated cellulose crystallites have a well-defined average distance. The changes observed from SAXS scattering curves are consistent with the well-defined packing of cellulose crystallites, and where this ordered packing is retained upon mild hydrolysis.

Transverse elastic modulus of T. pungens NC in order to have a better understanding of the mechanical properties of *T. pungens* nanocellulose, it is useful to investigate the transverse elastic modulus of individual NC particles. Since the 1930s, measuring the elastic properties of nanocellulose has been investigated by either experimental (wave propagation, X-ray diffraction, Raman spectroscopy, and AFM) or theoretical evaluation. Most of these studies have focused on measuring elastic modulus along the axial direction of the fibre (Cheng and Wang 2008; Guhados et al. 2005; Iwamoto et al. 2009; Lahiji et al. 2010; Tanaka and Iwata 2006; Tashiro and Kobayashi 1991), and only a few reports have concentrated on the transverse elastic modulus of an individual CNC using AFM or theoretical modelling (Jaswon et al. 1968; Lahiji et al. 2010; Pakzad et al. 2012; Tashiro and Kobayashi 1991). Theoretical modelling methods have predicted a transverse elastic modulus of 11–57 GPa for CNCs (Jaswon et al. 1968; Tashiro and Kobayashi 1991). Only a few studies calculated the transverse elastic modulus of CNCs based on the experimental data obtained via atomic force microscopy (AFM), and subsequently a physics-based model, where transverse elastic modulus values of 18–50 GPa for wood-derived CNCs (Lahiji et al. 2010), 24.8 and 17.7 GPa for wood and cotton CNCs respectively (Pakzad et al. 2012), and 2–25 GPa for tunicate CNCs have been estimated (Wagner et al. 2011; Wu et al. 2013).

In this work, the AM-FM (Amplitude Modulation-Frequency Modulation) method using AFM was applied to measure the transverse elastic modulus of *T. pungens* NC directly from the AFM image. AFM

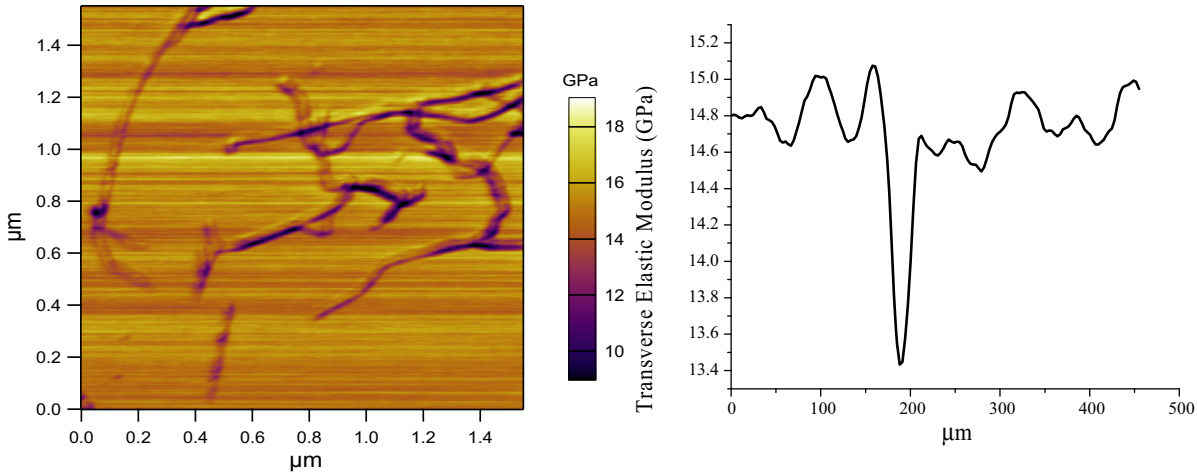

Fig. 9 Transverse elastic modulus of *T. pungens* NC measured by amplitude modulation–frequency modulation (AM–FM). *Top* topography image, *bottom* elastic modulus spectra

image and modulus spectra in Fig. 9 indicates that the transverse elastic modulus of *T. pungens* NC (with an average diameter of 3.45 ± 0.75 nm) obtained from an optimised acid hydrolysis process (40% (v/v) sulphuric acid, 45 °C, 3 h) is in the range of 8.5–14 GPa. In general, this transverse elastic modulus range is lower than previously-reported values and we postulate that this is because our spinifex-derived NC are indeed composites of crystalline cellulose and amorphous or paracrystalline hemicellulose (predominately xylose in our case).

Conclusions

In this study, we have demonstrated the isolation of unprecedentedly high aspect ratio nanocellulose from a non-wood source, Australian native biomass *T. pungens.* An optimised hydrolysis process for *T. pungens* was developed using sulphuric acid at low temperature (45 °C for 3 h) and low acid concentrations [40% (v/v)], which yielded high aspect ratio NC at 42% production yield, with an average crystallinity index of 73%. The average length of these NC particles was observed to be unaffected by intense ultrasonic treatments. A very high amount of hemicellulose retained in the bleached pulp acts as a less hydrolytically stable sacrificial interface during acid hydrolysis and this mechanism assists the retention of length of nanocellulose. The results from spectroscopic, thermal and X-ray crystallographic analysis also indicated the significant removal of lignin and amorphous polysaccharides upon pulping and hydrolysis. Finally, when benchmarked against previous work, the transverse elastic modulus of *T. pungens* NC has been found to be generally lower with respect to other common industry and laboratory sources of cellulose, and we suggest that this is due to the higher retained flexible hemicellulose content in these composite NC particles.

Acknowledgments The authors gratefully acknowledge the financial support from the Australian Research Council (under ARC Discovery Grant No. DP0877161). They also would like to acknowledge the Dugalunji Aboriginal Corporation in Camooweal for the project collaboration and the supply of spinifex grass samples. The authors acknowledge the University of Queensland, the Australian Microscopy and Microanalysis Research Facility at the Centre for Microscopy and Microanalysis for their facilities and technical assistance, as well as Dr Isabel Morrow for microscopy assistance. Finally, the authors would also like to thank Dr Elena Taran for the help with AM-FM analysis, which was performed at the Queensland node of the Australian National Fabrication Facility, a company established under the National Collaborative Research Infrastructure Strategy to provide nano and micro-fabrication facilities for Australian researchers. They also acknowledge the financial support (Proposal P3973) from ANSTO and Dr. Robert Knott for the scattering analysis.

References

Abdul Khalil HP, Davoudpour Y, Islam MN, Mustapha A, Sudesh K, Dungani R, Jawaid M (2014) Production and modification of nanofibrillated cellulose using various

mechanical processes: a review. Carbohydr Polym 99:649–665. doi:10.1016/j.carbpol.2013.08.069

Abraham E, Deepa B, Pothan LA, Jacob M, Thomas S, Cvelbar U, Anandjiwala R (2011) Extraction of nanocellulose fibrils from lignocellulosic fibres: a novel approach. Carbohydr Polym 86:1468–1475. doi:10.1016/j.carbpol.2011.06.034

Amiralian N, Annamalai PK, Memmott P, Martin DJ (2015a) Isolation of cellulose nanofibrils from Triodia pungens via different mechanical methods. Cellulose 22:2483–2498. doi:10.1007/s10570-015-0688-x

Amiralian N, Annamalai PK, Memmott P, Taran E, Schmidt S, Martin DJ (2015b) Easily deconstructed, high aspect ratio cellulose nanofibres from Triodia pungens; an abundant grass of Australia's arid zone. RSC Adv 5:32124–32132. doi:10.1039/C5RA02936H

Beck-Candanedo S, Roman M, Gray DG (2005a) Effect of reaction conditions on the properties and behavior of wood cellulose nanocrystal suspensions. Biomacromol 6:1048–1054. doi:10.1021/bm049300p

Beck-Candanedo S, Roman M, Gray DG (2005b) Effect of reaction conditions on the properties and behavior of wood cellulose nanocrystal suspensions. Biomacromol 6:1048–1054. doi:10.1021/bm049300p

Brinchia L, Cotanaa F, Fortunatib E, Kenny JM (2013) Production of nanocrystalline cellulose from lignocellulosic biomass: technology and applications. Carbohydr Polym 94:154–169

Camarero Espinosa S, Kuhnt T, Foster EJ, Weder C (2013) Isolation of thermally stable cellulose nanocrystals by phosphoric acid hydrolysis. Biomacromol 14:1223–1230. doi:10.1021/bm400219u

Cao X, Dong H, Li CM (2007) New nanocomposite materials reinforced with flax cellulose nanocrystals in waterborne polyurethane. Biomacromol 8:899–904. doi:10.1021/bm0610368

Cheng QZ, Wang SQ (2008) A method for testing the elastic modulus of single cellulose fibrils via atomic force microscopy. Compos Part A Appl Sci 39:1838–1843. doi:10.1016/j.compositesa.2008.09.007

Collard FX, Blin J (2014) A review on pyrolysis of biomass constituents: mechanisms and composition of the products obtained from the conversion of cellulose, hemicelluloses and lignin. Renew Sust Energ Rev 38:594–608. doi:10.1016/j.rser.2014.06.013

Crisp MD, Mant J, Toon A, Cook LG (2015) Australian spinifex grasses: new names in Triodia for Monodia and Symplectrodia. Phytotaxa 230:293–296

Cser F (2001) About the Lorentz correction used in the interpretation of small angle X-ray scattering data of semicrystalline polymers. J Appl Polym Sci 80:2300–2308. doi:10.1002/app.1335

Dias AS, Lima S, Pillinger M, Valente AA (2007) Modified versions of sulfated zirconia as catalysts for the conversion of xylose to furfural. Catal Lett 114:151–160. doi:10.1007/s10562-007-9052-6

Dussan K, Girisuta B, Lopes M, Leahy JJ, Hayes MH (2015) Conversion of hemicellulose sugars catalyzed by formic acid: kinetics of the dehydration of D-xylose, L-arabinose, and D-glucose. Chem Sus Chem 8:1411–1428. doi:10.1002/cssc.201403328

Eichhorn SJ (2011) Cellulose nanowhiskers: promising materials for advanced applications. Soft Matter 7:303–315. doi:10.1039/C0SM00142B

Elazzouzi-Hafraoui S, Nishiyama Y, Putaux JL, Heux L, Dubreuil F, Rochas C (2008) The shape and size distribution of crystalline nanoparticles prepared by acid hydrolysis of native cellulose. Biomacromol 9:57–65. doi:10.1021/bm700769p

Favier V, Chanzy H, Cavaille JY (1995) Polymer nanocomposites reinforced by cellulose whiskers. Macromolecules 28:6365–6367. doi:10.1021/ma00122a053

Fleming K, Gray DG, Matthews S (2001) Cellulose crystallites. Chemistry 7:1831–1835. doi:10.1002/1521-3765(20010504)7:9<1831:AID-CHEM1831>3.0.CO;2-S

French AD (2014) Idealized powder diffraction patterns for cellulose polymorphs. Cellulose 21:885–896

French AD, Santiago Cintron MS (2013) Cellulose polymorphy, crystallite size, and the Segal Crystallinity Index. Cellulose 20:583–588

Garcia de Rodriguez NL, Thielemans W, Dufresne A (2006) Sisal cellulose whiskers reinforced polyvinyl acetate nanocomposites. Cellulose 13:261–270. doi:10.1007/s10570-005-9039-7

Garvey CJ, Parker IH, Simon GP (2005) On the interpretation of X-ray diffraction powder patterns in terms of the nanostructure of cellulose I fibres. Macromol Chem Physic 206:1568–1575. doi:10.1002/macp.200500008

Gonzalez G, Lopez-Santin J, Caminal G, Sola C (1986) Dilute acid hydrolysis of wheat straw hemicellulose at moderate temperature: a simplified kinetic model. Biotechnol Bioeng 28:288–293. doi:10.1002/bit.260280219

Gu J, Catchmark JM (2012) Impact of hemicelluloses and pectin on sphere-like bacterial cellulose assembly. Carbohydr Polym 88:547–557. doi:10.1016/j.carbpol.2011.12.040

Guhados G, Wan W, Hutter JL (2005) Measurement of the elastic modulus of single bacterial cellulose fibers using atomic force microscopy. Langmuir 21:6642–6646. doi:10.1021/la0504311

Habibi Y, Hoeger I, Kelley SS, Rojas OJ (2010a) Development of Langmuir–Schaeffer cellulose nanocrystal monolayers and their interfacial behaviors. Langmuir 26:990–1001. doi:10.1021/la902444x

Habibi Y, Lucia LA, Rojas OJ (2010b) Cellulose nanocrystals: chemistry, self-assembly, and applications. Chem Rev 110:3479–3500. doi:10.1021/cr900339w

Hayashi N, Kondo T, Ishihara M (2005) Enzymatically produced nano-ordered short elements containing cellulose Iβ crystalline domains. Carbohydr Polym 61:191–197. doi:10.1016/j.carbpol.2005.04.018

He X et al (2014) Uniaxially aligned electrospun all-cellulose nanocomposite nanofibers reinforced with cellulose nanocrystals: scaffold for tissue engineering. Biomacromol 15:618–627. doi:10.1021/bm401656a

Henrique MA et al (2015) Kinetic study of the thermal decomposition of cellulose nanocrystals with different polymorphs, cellulose I and II, extracted from different sources and using different types of acids. Ind Crop Prod 76:128–140. doi:10.1016/j.indcrop.2015.06.048

Ilavsky J (2012) Nika: software for two-dimensional data reduction. J Appl Crystallogr 45:324–328. doi:10.1107/S0021889812004037

Ingegerd K, Atalla RH, Thompson NS (1995) Influence of hemicelluloses on the aggregation patterns of bacterial cellulose. Cellulose 2:129–144

Ioelovich M (2008) Cellulose as a nanostructured polymer: a short review. BioResources 3:1403–1418

Ioelovich M (2014) Peculiarities of cellulose nanoparticles. Tappi J 13:45–51

Iwamoto S, Kai W, Isogai A, Iwata T (2009) Elastic modulus of single cellulose microfibrils from tunicate measured by atomic force microscopy. Biomacromol 10:2571–2576. doi:10.1021/bm900520n

Jakob HF, Tschegg SE, Fratzl P (1996) Hydration dependence of the wood-cell wall structure in Picea abies. A small-angle X-ray scattering study. Macromolecules 29:8435–8440. doi:10.1021/ma9605661

Jaswon MA, Gillis PP, Mark RE (1968) The elastic constants of crystalline native cellulose. Proc R Soc Lond Ser A Math Phys Sci 306:389–412. doi:10.2307/2416113

Jorfi M, Roberts MN, Foster EJ, Weder C (2013a) Physiologically responsive, mechanically adaptive bio-nanocomposites for biomedical applications. ACS Appl Mater Interfaces 5:1517–1526. doi:10.1021/am303160j

Jorfi M, Roberts MN, Foster EJ, Weder C (2013b) Physiologically responsive, mechanically adaptive bio-nanocomposites for biomedical applications. Acs Appl Mater Inter 5:1517–1526. doi:10.1021/am303160j

Kaushik M, Moores A (2016) Review: nanocelluloses as versatile supports for metal nanoparticles and their applications in catalysis. Green Chem 18:622–637. doi:10.1039/c5gc02500a

Khandelwal M, Windle AH (2013) Self-assembly of bacterial and tunicate cellulose nanowhiskers. Polymer 54:5199–5206. doi:10.1016/j.polymer.2013.07.033

Krishnamachari P, Hashaikeh R, Chiesa M, El Rab KRMG (2012) Effects of acid hydrolysis time on cellulose nanocrystals properties: nanoindentation and thermogravimetric studies. Cell Chem Technol 46:13–18

Kumagai S, Matsuno R, Grause G, Kameda T, Yoshioka T (2015) Enhancement of bio-oil production via pyrolysis of wood biomass by pretreatment with H2SO4. Bioresour Technol 178:76–82. doi:10.1016/j.biortech.2014.09.146

Lahiji RR, Xu X, Reifenberger R, Raman A, Rudie A, Moon RJ (2010) Atomic force microscopy characterization of cellulose nanocrystals. Langmuir 26:4480–4488. doi:10.1021/La903111j

Lavoine N, Desloges I, Dufresne A, Bras J (2012) Microfibrillated cellulose–its barrier properties and applications in cellulosic materials: a review. Carbohydr Polym 90:735–764. doi:10.1016/j.carbpol.2012.05.026

Li RJ, Fei JM, Cai YR, Li YF, Feng JQ, Yao JM (2009) Cellulose whiskers extracted from mulberry: a novel biomass production. Carbohydr Polym 76:94–99. doi:10.1016/j.carbpol.2008.09.034

Lin N, Huang J, Dufresne A (2012) Preparation, properties and applications of polysaccharide nanocrystals in advanced functional nanomaterials: a review. Nanoscale 4:3274–3294. doi:10.1039/c2nr30260h

Lu P, Hsieh YL (2010) Preparation and properties of cellulose nanocrystals: rods, spheres, and network. Carbohydr Polym 82:329–336. doi:10.1016/j.carbpol.2010.04.073

Lu P, Hsieh YL (2012) Preparation and characterization of cellulose nanocrystals from rice straw. Carbohydr Polym 87:564–573. doi:10.1016/j.carbpol.2011.08.022

Lu QL, Tang LR, Lin FC, Wang SQ, Chen YD, Chen XR, Huang B (2014) Preparation and characterization of cellulose nanocrystals via ultrasonication-assisted FeCl3-catalyzed hydrolysis. Cellulose 21:3497–3506. doi:10.1007/s10570-014-0376-2

Mendez J, Annamalai PK, Eichhorn SJ, Rusli R, Rowan SJ, Foster EJ, Weder C (2011) Bioinspired mechanically adaptive polymer nanocomposites with water-activated shape-memory effect. Macromolecules 44:6827–6835. doi:10.1021/ma201502k

Mohammadinejad R, Karimi S, Iravani S, Varma RS (2016) Plant-derived nanostructures: types and applications. Green Chem 18:20–52. doi:10.1039/c5gc01403d

Mohd Amin KN, Annamalai PK, Morrow IC, Martin D (2015) Production of cellulose nanocrystals via a scalable mechanical method. RSC Adv 5:57133–57140. doi:10.1039/c5ra06862b

Moon RJ, Martini A, Nairn J, Simonsen J, Youngblood J (2011a) Cellulose nanomaterials review: structure, properties and nanocomposites. Chem Soc Rev 40:3941–3994. doi:10.1039/C0cs00108b

Moon RJ, Martini A, Nairn J, Simonsen J, Youngblood J (2011b) Cellulose nanomaterials review: structure, properties and nanocomposites. Chem Soc Rev 40:3941–3994. doi:10.1039/c0cs00108b

Moran JI, Alvarez VA, Cyras VP, Vazquez A (2008) Extraction of cellulose and preparation of nanocellulose from sisal fibers. Cellulose 15:149–159

Oksman K et al (2016) Review of the recent developments in cellulose nanocomposite processing. Compos Part A Appl Sci 83:2–18. doi:10.1016/j.compositesa.2015.10.041

Paakko M et al (2007) Enzymatic hydrolysis combined with mechanical shearing and high-pressure homogenization for nanoscale cellulose fibrils and strong gels. Biomacromol 8:1934–1941. doi:10.1021/bm061215p

Pakzad A, Simonsen J, Heiden PA, Yassar RS (2012) Size effects on the nanomechanical properties of cellulose I nanocrystals. J Mater Res 27:528–536. doi:10.1557/jmr.2011.288

Peng BL, Dhar N, Liu HL, Tam KC (2011) Chemistry and applications of nanocrystalline cellulose and its derivatives: a nanotechnology perspective. Can J Chem Eng 89:1191–1206. doi:10.1002/cjce.20554

Qing Y, Sabo R, Zhu JY, Agarwal U, Cai ZY, Wu YQ (2013) A comparative study of cellulose nanofibrils disintegrated via multiple processing approaches. Carbohydr Polym 97:226–234

Quievy N, Jacquet N, Sclavons M, Deroanne C, Paquot M, Devaux J (2010) Influence of homogenization and drying on the thermal stability of microfibrillated cellulose. Polym Degrad Stabil 95:306–314. doi:10.1016/j.polymdegradstab.2009.11.020

Rahimi M, Behrooz R (2011) Effect of cellulose characteristic and hydrolyze conditions on morphology and size of nanocrystal cellulose extracted from wheat straw. Int J Polym Mater 60:529–541. doi:10.1080/00914037.2010.531820

Roman M, Winter WT (2004) Effect of sulfate groups from sulfuric acid hydrolysis on the thermal degradation behavior of bacterial cellulose. Biomacromol 5:1671–1677. doi:10.1021/bm034519+

Rueda L, d'Arlas BF, Zhou Q, Berglund LA, Corcuera MA, Mondragon I, Eceiza A (2011) Isocyanate-rich cellulose nanocrystals and their selective insertion in elastomeric polyurethane. Compos Sci Technol 71:1953–1960. doi:10.1016/j.compscitech.2011.09.014

Sacui IA et al (2014) Comparison of the properties of cellulose nanocrystals and cellulose nanofibrils isolated from bacteria, tunicate, and wood processed using acid, enzymatic, mechanical, and oxidative methods. ACS Appl Mater Interfaces 6:6127–6138. doi:10.1021/am500359f

Saralegi A, Gonzalez ML, Valea A, Eceiza A, Corcuera MA (2014) The role of cellulose nanocrystals in the improvement of the shape-memory properties of castor oil-based segmented thermoplastic polyurethanes. Compos Sci Technol 92:27–33. doi:10.1016/j.compscitech.2013.12.001

Scheirs J, Camino G, Tumiatti W (2001) Overview of water evolution during the thermal degradation of cellulose. Eur Polym J 37:933–942. doi:10.1016/S0014-3057(00)00211-1

Scherrer P (1918) Bestimmung der Grösse und der inneren Struktur von Kolloidteilchen mittels Röntgenstrahlen. Nachr Ges Wiss Göttingen 26:98–100

Segal L, Creely JJ, Martin AE, Conrad CM (1959) An empirical method for estimating the degree of crystallinity of native cellulose using the X-ray diffractometer. Text Res J 29:786–794. doi:10.1177/004051755902901003

Sheltami RM, Abdullah I, Ahmad I, Dufresne A, Kargarzadeh H (2012) Extraction of cellulose nanocrystals from mengkuang leaves (*Pandanus tectorius*). Carbohydr Polym 88:772–779. doi:10.1016/j.carbpol.2012.01.062

Tanaka F, Iwata T (2006) Estimation of the elastic modulus of cellulose crystal by molecular mechanics simulation. Cellulose 13:509–517. doi:10.1007/s10570-006-9068-x

Tashiro K, Kobayashi M (1991) Theoretical evaluation of three-dimensional elastic constants of native and regenerated celluloses: role of hydrogen bonds. Polymer 32:1516–1526

Teixeira ED, Correa AC, Manzoli A, Leite FL, de Oliveira CR, Mattoso LHC (2010) Cellulose nanofibers from white and naturally colored cotton fibers. Cellulose 17:595–606. doi:10.1007/s10570-010-9403-0

Tonoli GH, Teixeira EM, Correa AC, Marconcini JM, Caixeta LA, Pereira-da-Silva MA, Mattoso LH (2012) Cellulose micro/nanofibres from Eucalyptus kraft pulp: preparation and properties. Carbohydr Polym 89:80–88. doi:10.1016/j.carbpol.2012.02.052

Toon A, Crisp MD, Gamage H, Mant J, Morris DC, Schmidt S, Cook LG (2015) Key innovation or adaptive change? A test of leaf traits using Triodiinae in Australia. Sci Rep 5:12398. doi:10.1038/srep12398

Wagner R, Moon R, Pratt J, Shaw G, Raman A (2011) Uncertainty quantification in nanomechanical measurements using the atomic force microscope. Nanotechnology 22:455703. doi:10.1088/0957-4484/22/45/455703

Wang N, Ding EY, Cheng RS (2007) Thermal degradation behaviors of spherical cellulose nanocrystals with sulfate groups. Polymer 48:3486–3493. doi:10.1016/j.polymer.2007.03.062

Werner K, Pommer L, Brostrom M (2014) Thermal decomposition of hemicelluloses. J Anal Appl Pyrol 110:130–137. doi:10.1016/j.jaap.2014.08.013

Wu XW, Moon RJ, Martini A (2013) Crystalline cellulose elastic modulus predicted by atomistic models of uniform deformation and nanoscale indentation. Cellulose 20:43–55. doi:10.1007/s10570-012-9823-0

Yang HP, Yan R, Chen HP, Lee DH, Zheng CG (2007) Characteristics of hemicellulose, cellulose and lignin pyrolysis. Fuel 86:1781–1788. doi:10.1016/j.fuel.2006.12.013

Yin Y, Berglund L, Salmen L (2011a) Effect of steam treatment on the properties of wood cell walls. Biomacromol 12:194–202. doi:10.1021/bm101144m

Yin Y, Berglund L, Salmén L (2011b) Effect of Steam Treatment on the Properties of Wood Cell Walls. Biomacromol 12:194–202. doi:10.1021/bm101144m

Yoon SY, Han SH, Shin SJ (2014) The effect of hemicelluloses and lignin on acid hydrolysis of cellulose. Energy 77:19–24. doi:10.1016/j.energy.2014.01.104

Yue YY, Zhou CJ, French AD, Xia G, Han GP, Wang QW, Wu QL (2012) Comparative properties of cellulose nanocrystals from native and mercerized cotton fibers. Cellulose 19:1173–1187. doi:10.1007/s10570-012-9714-4

Zhao HB, Kwak JH, Zhang ZC, Brown HM, Arey BW, Holladay JE (2007) Studying cellulose fiber structure by SEM, XRD, NMR and acid hydrolysis. Carbohydr Polym 68:235–241. doi:10.1016/j.carbpol.2006.12.013

Zhao Y, Zhang Y, Lindstrom ME, Li J (2015) Tunicate cellulose nanocrystals: preparation, neat films and nanocomposite films with glucomannans. Carbohydr Polym 117:286–296. doi:10.1016/j.carbpol.2014.09.020